Penning and associative ionization of mercury by collision with metastable rare gas atoms

L. Appolloni, B. Brunetti, J. Hermanussen, F. Vecchiocattivi, and G. G. Volpi

Citation: The Journal of Chemical Physics **87**, 3804 (1987); doi: 10.1063/1.452936
View online: http://dx.doi.org/10.1063/1.452936
View Table of Contents: http://scitation.aip.org/content/aip/journal/jcp/87/7?ver=pdfcov
Published by the AIP Publishing

Penning and associative ionization of mercury by collision with metastable rare gas atoms

L. Appolloni, B. Brunetti, J. Hermanussen, F. Vecchiocattivi, and G. G. Volpi
Dipartimento di Chimica dell'Università 06100 Perugia, Italy

(Received 18 February 1987; accepted 27 May 1987)

The ionization of mercury atoms by thermal energy collisions with metastable neon, argon, and krypton has been studied in a crossed beam experiment. The production of both Hg^+ and RHg^+ (R = Ne, Ar, Kr) ions has been observed and the collision energy dependence of the cross section for each ionization channel has been measured. The experimental relative cross sections have also been analyzed in terms of an optical model. In all cases the main ionic product is the Hg^+ ion. The average relative yield of RHg^+ appears to increase going from neon to krypton. The different role of the two spin–orbit states of the metastable krypton atoms has been assessed: The $Kr(^3P_0)$ atoms can produce both Hg^+ and $KrHg^+$ in the whole energy range investigated, while the $Kr(^3P_2)$ atoms can ionize the mercury only for a collision energy larger than ~0.15 eV, producing $KrHg^+$ in the energy range between ~0.15 and ~0.5 eV, and producing also Hg^+ at energies larger than ~0.5 eV.

I. INTRODUCTION

The ionization processes which can occur in the collision between an excited rare gas atom, R*, and a mercury atom can lead to the production of Hg^+ or RHg^+:

$$R^* + Hg \rightarrow R + Hg^+ + e^-$$
$$\rightarrow RHg^+ + e^- .$$

The first process is usually called "Penning ionization" (PI), while the second one "associative ionization" (AI).

More than 20 years ago Herman and Cermak[1] observed in a mass-spectrometric experiment the production of Hg^+ and RHg^+ ions (R = Ar, Kr, and Xe) due to the collisions between metastable rare gas and mercury atoms. Since this early work only a few papers have been devoted to the study of these processes, in spite of their importance in several practical applications such as thermal plasmas, electrical discharges, etc. The collision energy dependence of the total ionization cross section for collisions of He*, Ne*, and Ar* with Hg has been measured by Illenberger and Niehaus,[2] while Hotop *et al.*[3] have studied the energy spectrum of the electrons produced in the ionization of mercury by collisions with *J*-selected metastable neon atoms. Burgmans *et al.*[4] have recently reported ionization coefficients for a discharge of rare gas–mercury mixtures. However, the relative importance of AI and PI never has been investigated accurately until the recent crossed beams experiment performed in our laboratory[5] which showed the different role played, at low collision energy, by the two spin–orbit states of metastable krypton atoms.

The energy transfer process between $Kr^*(^3P_2)$ and Hg leading to $Hg^*(6\,^3P_1)$ has been studied in a crossed beams experiment by Lee and Martin,[6] while the rate constants for the quenching of metastable rare gases by mercury have been measured by Wren and Setser.[7]

From the studies mentioned above it is now clear that ionization occurs predominantly in collisions involving He*, Ne*, and Ar*, which have an excitation energy larger than the ionization potential of mercury (10.43 eV). For Kr* the recent work performed in our laboratory[5] has shown that the $^3P_0$ state of Kr* leads to both PI and AI processes, while, in the thermal energy range, the $^3P_2$ state can produce only the $KrHg^+$ ion after a threshold energy of about 0.15 eV. In the present paper we study the cross sections for PI and AI processes for collisions of Ne* and Ar* with Hg and in addition we extend the study of the ionization by Kr* up to about 1 eV collision energy, in order also to observe the threshold for the PI process due to the $Kr^*(^3P_2)$ atoms. The experimental data have been obtained in a crossed beam apparatus, analyzing the product ions by mass spectrometry and measuring the collision velocity dependence by a time-of-flight technique. The results have also been analyzed in terms of an optical model in order to obtain information about the potential energy functions involved in the processes.

II. THE EXPERIMENTAL APPARATUS

The crossed beams apparatus used for obtaining the present experimental results is the same which was previously described for other studies.[5,8–10] Only a general description is given here with some details about the modifications introduced for the present experiment.

A beam of metastable rare gas atoms crosses at right angle a beam of mercury atoms. The ions produced in the beam crossing region are extracted by an electric field, focused by an electrostatic lens system, analyzed by a quadrupole mass filter, and then detected. A schematic view of the experimental setup is shown in Fig. 1.

The rare gas beam is produced by an effusive source with a round slit of about 1 mm diam filled with a few Torr pressure of rare gas. After collimation the beam crosses an electron bombardment exciter. The electrons come from a hot tungsten filament and are accelerated by applying a positive potential of 500 V to a rectangular plate anode placed at about 2 cm. After the exciter the beam passes through an electric field of 1.6 KV/cm, which removes the ions and quenches the high Rydberg states, probably also produced by the bombarding electrons.

 0021-9606/87/193804-08$02.10

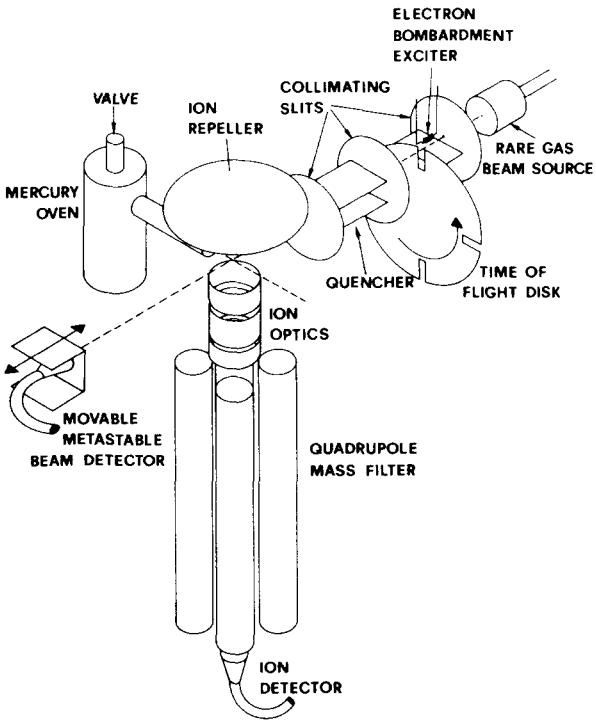

FIG. 1. A schematic view of the experimental setup.

The target mercury beam is produced by a glass microcapillary array connected to an oven heated at about 450 K. Since the mercury vapor in the vacuum background pressure can seriously damage the channel electron multipliers used to detect the product ions and the metastable atoms, some expedients have been used in order to maintain a low concentration of mercury in the ambient gas. A valve can separate the oven from the multicapillary array in order to open the beam only during the measurement. Moreover, a liquid nitrogen cooled plate is placed in front of the target beam just after the crossing center to trap the mercury atoms.

From the crossing volume the product ions are extracted at an energy of about 250 eV. The size of the crossing volume and the extracting voltage both insure that the ion detection efficiency for different masses does not depend on the collision energy. Previous experiments on other systems with the present crossed beam configuration[9,10] have shown a good agreement with the results obtained in other laboratories with different techniques.

The ions are mass analyzed by a quadrupole mass filter having a mass range from 1 to about 1000. The resolution has been adjusted to have a compromise between a satisfying separation between the atomic and molecular ions and a good signal intensity.

The metastable atoms are dectected by a channel electron multiplier which can be moved into the scattering center when desired. This allows measuring the metastable atom time-of-flight spectra directly in the reaction volume.

Time-of-flight spectra are obtained by pulsing the metastable atom beam with a slotted disk. The pulses can have an adjustable frequency ranging from 350 to 3500 Hz. In the present case a frequency of about 1600 Hz has been used, which corresponds to a gate opening time of about 40 μs. The distance between the scattering center and the slotted disk is about 16 cm. The pulses for the metastable atoms or for the product ions, coming from the detector, are preamplified, amplified, discriminated and then sent, together with the start pulses, to a computer controlled CAMAC unit data acquisition system based on a high-speed multichannel scaler and a PDP 11/23 unit. The time spectra for the product ions are then corrected for the ion flight time and the transmission throughout the mass filter. Typical time spectra for metastable krypton atoms, Hg^+ and $KrHg^+$ ions are reported in Fig. 2. For the spectra of the figure the pulses have been counted for 180 s. A small peak due to ultraviolet photons is well evident in the spectrum of Kr*. These photons come from the exciter region and their peak is very useful both for the calibration of the zero on the time scale and for a direct measurement of the resolution function of the time-of-flight system.

The $^3P_2/^3P_0$ concentration ratio in the metastable rare gas beams was not measured, but is expected to be approximately the statistical ratio 1/5.[6]

III. RESULTS

In Fig. 3 the cross sections for Hg^+ ion formation in collisions between Ne* and Hg are reported for the energy range investigated in the present work. The associate ions $NeHg^+$ are also produced, with an average AI to PI cross section ratio of about 0.03. The velocity dependence of the AI cross section was not measured because of the low intensity of the $NeHg^+$ product ions. On the other hand since the AI is relatively lower than the statistical error for the PI data ($\sim$10%), the cross sections of Fig. 3 are expected to be rather close to the total ionization cross sections. In Fig. 4 the present PI cross sections are plotted together with the total ionization cross sections for this system reported by Illenberger and Niehaus.[2] A substantial agreement exists between the two sets of cross sections.

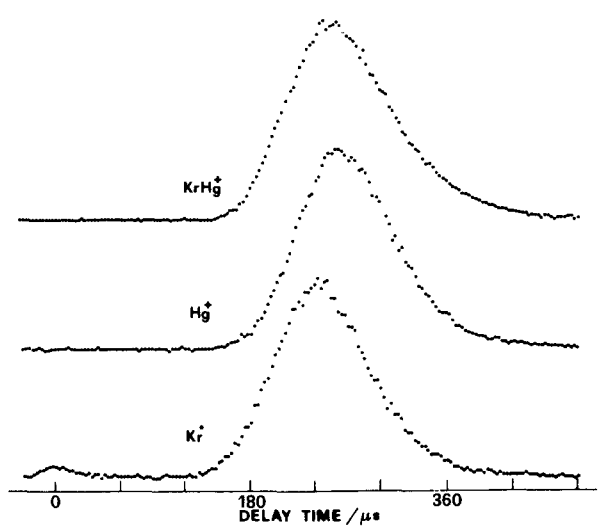

FIG. 2. Typical time spectra for Kr*, Hg^+, and $KrHg^+$. The small peak around zero delay time in the Kr* spectrum is due to ultraviolet photons produced in the electron bombardment exciter.

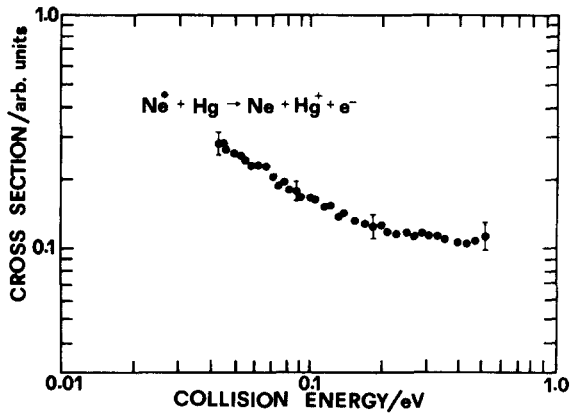

FIG. 3. Collision energy dependence for the Penning ionization cross section in Ne*–Hg collisions. The bars indicate some typical statistical errors.

In Fig. 5 the PI and AI cross sections are shown as a function of the collision energy for the Ar* + Hg system. Also for this system the total ionization cross section $\sigma_T = \sigma_{AI} + \sigma_{PI}$ had been previously reported by Illenberger and Niehaus[2]: In Fig. 6 the present σ_T results and those previously reported are compared and appear in a good agreement. The branching ratio, σ_{AI}/σ_T, is also plotted in the figure.

In Fig. 7 the AI and PI cross sections for the Kr* + Hg system, up to about 0.5 eV, are reported, while the branching ratio up to an energy of about 1 eV is reported in Fig. 8. The higher energy measurement has been performed under different experimental conditions: The metastable krypton atoms were produced in a seeded supersonic beam. A 0.1 mm slit was used for the beam source, with about 200 Torr pressure of a H_2/Kr mixture with about 5% of krypton. In this way velocities higher than those from the effusive source were obtained, and for each velocity the $KrHg^+/Hg^+$ intensity ratio can be easily measured. However, only the branching ratio has been satisfactorily obtained for the high energy range mostly because of the low resolution of the present time-of-flight configuration. On the other hand the second

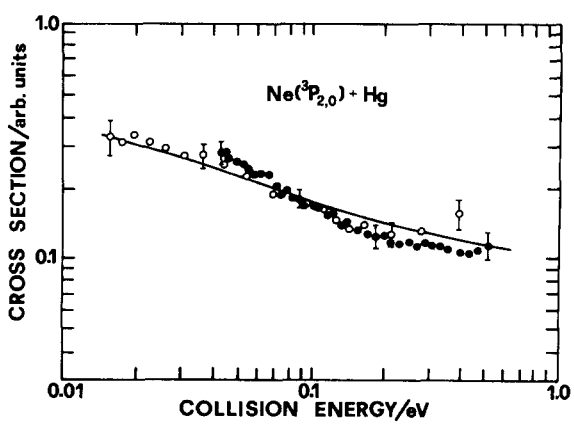

FIG. 4. Penning ionization cross sections of Fig. 3 (full circles) and the total ionization cross sections of Ref. 2 (open circles) for the Ne*–Hg collisions. The curve is the total ionization cross section calculated within the optical model.

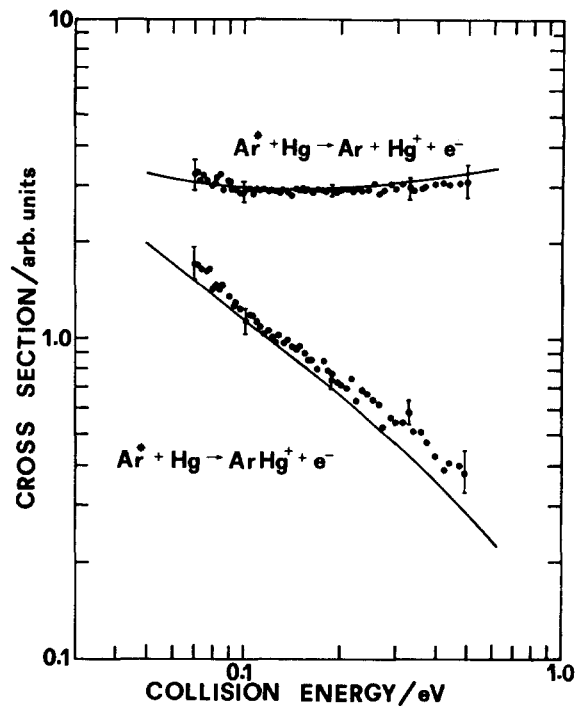

FIG. 5. Collision energy dependence of the Penning and associative ionization cross sections in Ar*–Hg collisions. The cross section scale is in arbitrary units, but the relative value of the associative and Penning ionization cross sections is that one experimentally determined, with an uncertainty of ~20%. The bars indicate some typical statistical errors. The curves are the best fit calculation performed within the optical model.

threshold in the energy dependence of the ionization cross section appears well evident in the branching ratio. A test performed with pure H_2 beams has shown that the presence of hydrogen in the beam does not affect the ion production.

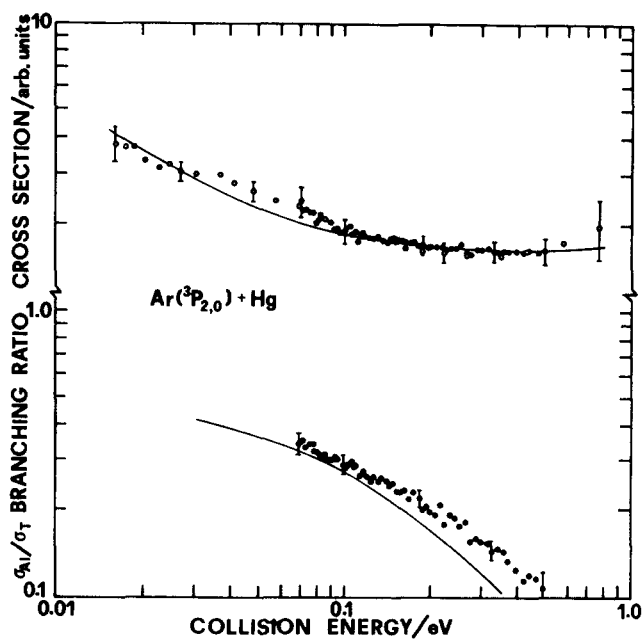

FIG. 6. Total ionization cross sections from Ref. 2 (open circles) and those from the present work (full circles) for Ar*–Hg collisions. The associative to total ionization cross section ratio is also reported. The curves are the best fit calculation performed within the optical model.

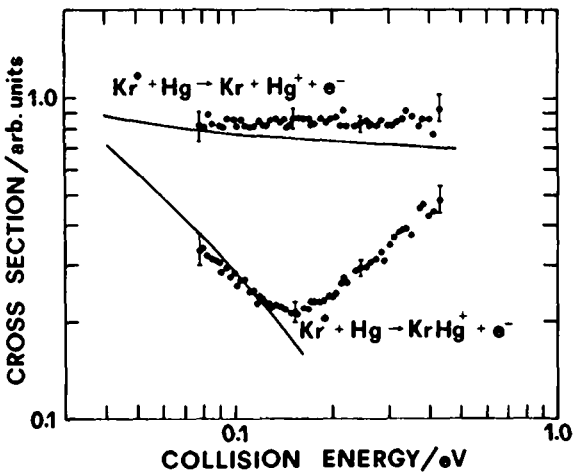

FIG. 7. Collision energy dependence of the Penning and associative ionization cross sections in Kr*–Hg collisions. The cross section scale is in arbitrary units, but the relative value of the associative and Penning ionization cross sections is that one experimentally determined, with an uncertainty of ~20%. The bars indicate some typical statistical errors. The curves are the best fit calculation, within the optical model, for the $Kr^*(^3P_0)$ state.

IV. OPTICAL MODEL ANALYSIS

In this section we report the results of an analysis of the ionization cross sections in Ne*, Ar*, and Kr* collisions with Hg, performed under the assumption of an optical potential describing the interaction between the two colliding partners.

A. The theoretical model

It is well known that the ionization processes, like those studied in the present work, can be attributed to the transition between a discrete state, representing the reacting particles, and the continuum of states representing the final ion with a free electron. The optical model which is usually assumed for the description of these ionization phenomena implies a complex potential

$$W(R) = V(R) - i/2\Gamma(R)$$

whose real part, $V(R)$, describes the interaction between the colliding particles and the imaginary part, $-\Gamma(R)/2$, is responsible for the coupling with the ionization continuum. A theoretical treatment of PI and AI processes within this model is available in the literature[11-16] and just few points relevant to the present analysis are reported here.

In Fig. 9 two cases are schematically drawn: a case (a), where the curve describing the interaction between the reacting particles, $V(R)$, is always embedded into the ionization continuum; and a case (b) where the $V(R)$ curve penetrates the continuum only at distances shorter than R_C. We will see below that the case (a) is that of the Ne*, Ar*, $Kr^*(^3P_0)$–Hg systems, while $Kr^*(^3P_2)$–Hg is represented by the case (b). From a semiclassical picture of the process of type (a)[12,13] it has been obtained for the total ionization cross section, σ_T, at a given relative velocity, v,

$$\sigma_T(v) = 2\pi \int_0^\infty P_T(b,v) b\, db\,,$$

where b is the classical impact parameter and $P_T(b,v)$ is the probability for total ionization given by

$$P_T(b,v) = 1 - \exp\left[-2 \int_{R_0(b)}^\infty \Gamma(R) dR / h v_r(R) \right],$$

where $R_0(b)$ is the classical turning point and $v_r(R)$ is the radial velocity given by

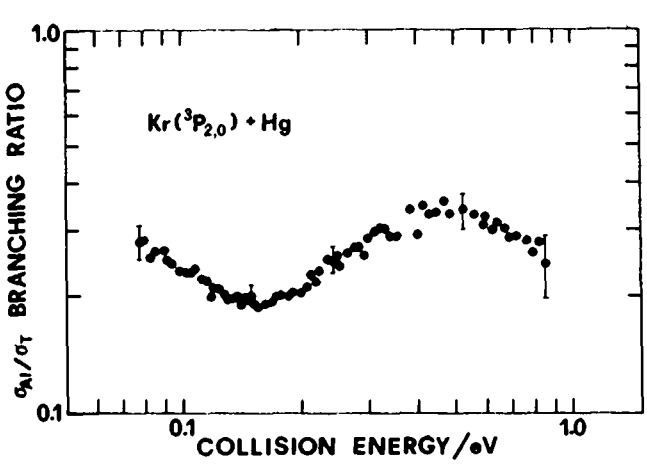

FIG. 8. Associative to total ionization cross section ratio for the Kr*–Hg collisions. The two changes in slope occur at the threshold energies for the $Kr^*(^3P_2)$ state: the first one for the $KrHg^+$ ion production and the second one for the Hg^+ ion production.

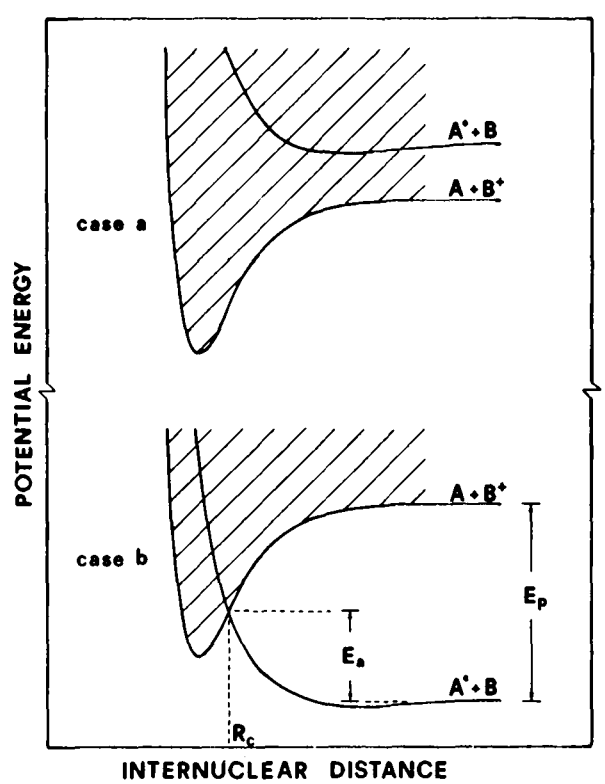

FIG. 9. The two typical situations for the ionization in A^*–B collisions. Case (a): The $A^* + B$ potential energy curve is always embedded in the $A + B^+ + e^-$ continuum. Case (b): The $A^* + B$ potential energy curve penetrates the $A + B^+ + e^-$ continuum at distances shorter than R_C and for collision energy larger than E_a.

$$v_r(R) = v[1 - V(R)/E - (b/R)^2]^{1/2} .$$

For the σ_{AI} we have

$$\sigma_{AI}(v) = 2\pi \int_0^\infty P_{AI}(b,v) b\, db ,$$

with

$$P_{AI}(b,v) = \left\{1 - \exp\left[-2 \int_{R_0(b)}^{R_A(b)} \Gamma(R) dR / h v_r(R) \right]\right\} \times \exp\left[- \int_{R_A(b)}^{\infty} \Gamma(R) dR / h v_r(R) \right] .$$

$R_A(b)$ is the limiting distance for the associative ionization, such that

$$V(R_A) - E = V_+(R_A) - H(b) ,$$

where $V_+(R)$ and $H(b)$ are, respectively, the potential energy curve and the height of the centrifugal barrier for the final diatomic ion system.

The presence of $H(b)$ implies that all the metastable diatomic ions produced in the ionization are also considered for the σ_{AI}. Actually the lifetime of these metastable diatomic ions has to be compared with the detection time in our experiment. The latter is given essentially by the ion flight time of the ion throughout the mass filter which is of the order of 10^{-5} s. The lifetime of the metastable diatomic ions depends on their probability for tunneling through the centrifugal barrier. This lifetime has been calculated for some typical situations occurring in the systems studied here by using semiclassical formulas[17] and the potential curves described in the next section. For the present processes we have found that the average lifetime of the metastable diatomic product ions is always shorter than 10^{-8} s. Therefore in the present experiment we detect only the atomic ions produced by the predissociation of these metastable diatomic ions. Naturally we cannot distinguish these ions from the Penning ions. Therefore in our analysis we have completely neglected $H(b)$ making R_A independent on the impact parameter.

The case (b) has been also already considered theoretically.[14,15] In this situation we have two threshold energies: For a collision energy $E < E_a$ ionization cannot occur; for $E_a < E < E_p$ (see Fig. 9) only AI can occur, while for $E > E_p$ both AI and PI occur. The total cross section in the two ionization energy ranges is

$$\sigma_T(v) = 2\pi \int_0^\infty P_T(b,v) b\, db ,$$

with

$$P_T(b,v) = 1 - \exp\left[-2 \int_{R_0(b)}^{R_C} \Gamma(R) dR / h v_r(R) \right] .$$

For $E_a < E < E_p$ we have $P_{AI} = P_T$ and for $E > E_p$

$$P_{AI}(b,v) = \left\{1 - \exp\left[-2 \int_{R_0(b)}^{R_A} \Gamma(R) dR / h v_r(R) \right]\right\} \times \exp\left[- \int_{R_A}^{R_C} \Gamma(R) dR / h v_r(R) \right] .$$

All these semiclassical expressions have been used to analyze the present experimental data.

B. The potential energy curves

To calculate the ionization cross section following the procedure mentioned in the previous section one needs a curve $V(R)$, the imaginary component $\Gamma(R)$, and, for the AI cross section, also the $V_+(R)$ ion curve.

In Fig. 10 the energy levels for the excited rare gas atoms, the mercury ion, and the zero point energy of the associate ions are reported. From the energy levels of the systems involved in the processes studied, it can be observed that the metastable atoms are all in a ^3P state with 0 and 2 spin–orbit components. These atoms interact with the ground state Hg atom with an anisotropic potential[9,18] leading, for the $^3P_0$ and $^3P_2$, respectively, to one and three adiabatic potential energy curves.[9] However, it must be considered that these atoms can be seen as halogen-like ions surrounded by s-orbital valence electrons. Their anisotropy should be lower than that exhibited by the halogen atoms[19] because of the different nuclear charge. Moreover, the distances probed by the collision energies of this experiment are never shorter than ~ 3 Å. It follows that for the present collisional phenomena the core anisotropy does not affect too much the interaction, and spherically symmetric potentials can be reasonably assumed for the interaction between Ne*, Ar*, Kr*, and Hg. Direct information about these potential curves are not available. However from the above arguments it appears appropriate to approximate these curves to those of the corresponding alkali–Hg systems.

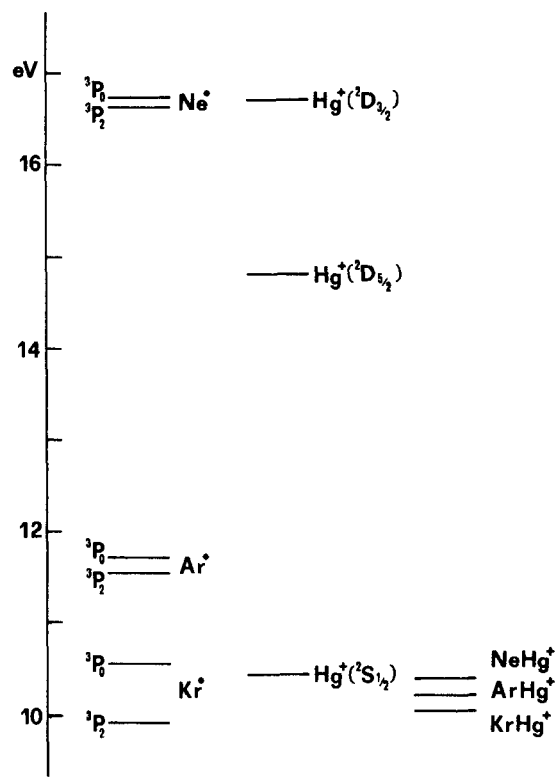

FIG. 10. Atomic energy levels for the metastable rare gas and the mercury atom relevant to Penning and associative ionization processes. The zero point energy levels for the ground state associate ions are also reported.

For Ne*–Hg we have used the potential curve given by Buck and Pauly[20] from the inversion of scattering data for the Na–Hg system. For Ar*–Hg we have used the recent potential by Lackschwitz *et al.*[21] for a K–Hg system, also obtained from the inversion of differential elastic cross sections. A potential curve, of the same quality, for Rb–Hg, which could be used for the analysis of a Kr*–Hg system, is not available. However, the K–Hg and Cs–Hg potential curves are rather similar,[22] therefore we have used for Kr*–Hg a curve with the same reduced shape of that one for K–Hg, but scaled using the ratios for the potential minimum and the equilibrium distance of K–Hg and Rb–Hg determined by Barwig *et al.*[23] from differential cross sections. In Table I the characteristics of the potential curves used in the present analysis are summarized.

The final R–Hg^+ ions are in a $^2\Sigma$ state and we have used for their potential curves a Morse function

$$V_+(R) = D_e(y^2 - 2y)\,,$$

$$y = \exp[\,-\beta(R/R_e - 1)\,]\,,$$

assuming for $ArHg^+$ the R_e and β values from spectroscopy[24] and the D_e value from the photoionization spectrum by Linn *et al.*[25] For $KrHg^+$ we have assumed the D_e value from the recent photoionization experiment by Liao and Ng[26] and the R_e obtained from the correlation rules by Liuti and Pirani[27] adapted to a $\sim R^{-4}$ long range attraction. The characteristics of these potential curves are also summarized in Table I.

C. Analysis of the experimental data

In Fig. 4 the present results and those by Illenberger and Niehaus[2] for the total ionization cross section in Ne*–Hg collisions are compared with the calculation performed by using the imaginary component of the optical potential obtained by Gregor and Siska[28] for the Ne*–Xe system. Experiments and calculation appear in good agreement; actually Xe and Hg both have similar atomic sizes as indicated by their polarizabilities which are also similar.

We have performed a calculation also of the AI cross section assuming for $NeHg^+$ a potential dissociation energy of 50 meV and an equilibrium distance of 2.5 Å, which are values roughly similar to those of the $NeXe^+$.[29] The average AI cross section calculated is about 2% of the PI one, that is rather close to the experimental results. However, it should be noted that the Ne* can produce Hg^+ also in two excited states, and therefore this calculation has only an indicative meaning. The presence of excited Hg^+ states in the ionization of Hg by Ne* has been observed by Hotop *et al.*[3] who measured the electron energy spectrum in J-selected collisions.

In Fig. 11 the potential energy curves for Ar*–Hg interaction together with that for Ar–Hg^+ are reported. For this system we have calculated the cross sections assuming an exponential function for the imaginary component of the optical potential

$$\Gamma(R) = A\exp(-sR)$$

whose parameters have been adjusted to have good fit of the experimental total cross sections and of branching ratios. The best-fit values are $A = 624$ eV and $s = 3.2$ Å^{-1}. In Fig. 5 and Fig. 6 the calculated cross sections are reported together with the experimental data.

In Fig. 11 the potential energy curves relevant to the Kr*–Hg system are also reported. For this system we can distinguish two regions: In the energy range up to $\sim$0.15 eV the cross sections are due to the $^3P_0$ state only, because for the $^3P_2$ the ionization is not energetically accessible; for energies higher than $\sim$0.15 eV both the $^3P_0$ and $^3P_2$ states of Kr* contribute to the ionization. In a first step we have considered for the analysis the cross sections for the $^3P_0$ state only. Also in this case we have adjusted the A and s parameters of the exponential function for the imaginary component $\Gamma(R)$ to obtain a good fit of the experimental data. The best fit cross sections for Kr*($^3P_0$) collisions are reported in Fig. 7 and the best-fit parameters are $A = 811$ eV and $s = 2.85$ Å^{-1}.

Further we have tried to fit the energy dependence of the branching ratio by considering also the cross section of the $^3P_2$ state of Kr* and combining the two contributions through the $^3P_0/^3P_2$ population ratio. An acceptable fit both of the shape and of the threshold energies with the present potential energy curves was not obtained. In the next section it will be shown that this is a consequence of the presence of a manifold of potential curves penetrating the continuum.

TABLE I. Some characteristics of the potential energy curves used for the calculation of the ionization cross sections.

	D_e (meV)	R_e (Å)
Ne*–Hg	54.9	4.79
Ar*–Hg	52.4	4.91
Kr*–Hg	51.2	4.94
Ar–Hg^+	228.0	2.87
Kr–Hg^+	393.0	2.97

V. DISCUSSION

The original contribution of the present work relatively to the previous ones on this subject is the systematic study of the energy dependence of the single ionization channels (AI and PI) of Hg by metastable rare gases. A first remarkable result is the observation of an increase in the branching ratio when passing from Ne* to Kr*. This trend can be understood looking at the nature of the bond in the final R–Hg^+ molecule. The photoionization experiments by Ng and coworkers[25,26] on the rare gas–mercury van der Waals molecules have shown that the bond energy of the RHg^+ ions increases in the sequence $ArHg^+$, $KrHg^+$, and $XeHg^+$. Moreover, this increase reflects rather well the increase in the rare gas polarizability, indicating that the bond is mainly dominated by the long range ion-induced dipole interaction. Therefore, the higher AI contribution to the total ionization with heavier metastable rare gas atoms is simply due to a stronger R–Hg^+ bond.

Wren and Setser[7] have reported the quenching rate constants, measured at room temperature, for metastable rare gas atoms in mercury. We have calculated the ionization rate constants at room temperature by using the total ionization

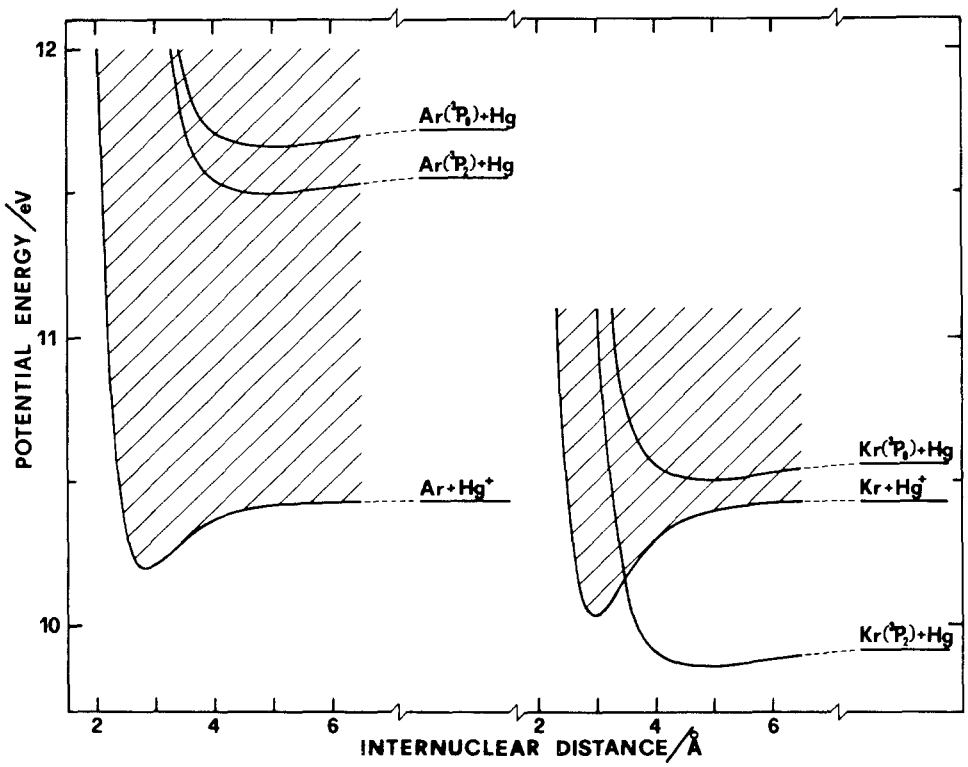

FIG. 11. Potential energy curves for the interaction between the two metastable states of argon and krypton atoms with mercury atoms and those for the related ions. The case of the Kr*($^3P_2$)–Hg system is of type (b) while the other cases are of type (a) (see Fig. 9).

cross sections obtained from the present best-fit optical potentials for Ne* and Ar*–Hg and averaging over the Maxwell–Boltzmann distribution at room temperature. We have obtained the values 1.47×10^{-10} and 2.19×10^{-10} $cm^3\ s^{-1}$ molecule^{-1} for the ionization rate constants of Ne* and Ar*–Hg, respectively, while the quenching rate constants by Wren and Setser[7] are, respectively, 4.11×10^{-10} and 8.67×10^{-10} $cm^3\ s^{-1}$ molecule^{-1}.[30] Considering the assumptions made for the calculation, the agreement within the order of magnitude of these ionization rate constants with the experimental ones for the quenching confirms that the ionization is an important channel in the quenching of Ne* and Ar* by Hg. The experimental quenching rate constant reported by Wren and Setser[7] for Kr* is for the $^3P_2$ state only and therefore a comparison cannot be given because, as is discussed below, this state can be quenched in two ways in different collision energy regions: by electronic energy transfer and/or by ionization.

The two extrema in the branching ratio for Kr*–Hg indicate two threshold energies: The first one for AI[5] and the second one for PI, both due to the Kr*($^3P_2$)–Hg collisions. The value of the threshold E_a (see Fig. 9) evaluated from the potential energy curves discussed in Sec. IV B (see Fig. 11) is about 0.24 eV, while the present experimental threshold for AI in Kr*($^3P_2$)–Hg collisions is about 0.15 eV. On the other hand, the experimental threshold for PI in Kr*($^3P_2$)–Hg appears to be rather close to the expected E_p value of 0.51 eV. The first threshold is lower than that expected from potential curves, but is very close to the difference between the 9.92 eV electronic energy of Kr*($^3P_2$) and the zero point vibrational energy of Kr–Hg$^+$. Actually, from the atomic energy levels of Hg[31] it can be seen that between 9.92 eV and the E_a energy many excited Hg states exist and one of them (the 9 $^1P_1$ state) is quasiresonant with Kr*($^3P_2$)–Hg. This shows that the Kr*($^3P_2$)–Hg curve, before penetrating the ionization continuum, has the possibility of crossing several Kr–Hg** curves with possible nonadiabatic effects. In other words, when Kr*($^3P_2$) collides with Hg, at an energy lower than the ionization threshold, a Rydberg Hg** state can be produced[32] and this highly excited atom can cascade down, for instance to Hg*($6\,^3P_1$) whose characteristic decay radiation has been observed.[6,7] When the energy is sufficiently high the system penetrates the ionization continuum, but in most part along one of the many Kr–Hg** curves, which could be less repulsive being Hg** a "rather soft" atom. In such a case the E_a value becomes lower than that expected for the Kr*–Hg curve, and this explains the lower threshold for AI which has been observed. Obviously the second threshold E_p is not affected by the potential energy curves being determined only by the asymptotic energy levels. In fact the experimental second threshold ($\sim$0.5 eV) is in very good agreement with that expected (0.51 eV).

Since the Kr*($^3P_2$)–Hg system does not arrive into the ionization continuum traveling along one well-defined potential curve, the failure of the optical model in this case is understandable. On the other hand for the other systems, Ne*, Ar*, Kr*($^3P_0$)–Hg, the optical model appears to be adequate in the investigated energy range.

VI. CONCLUSIONS

The energy dependence and the relative values of the cross sections for AI and PI in mercury–metastable rare gas atom collisions have been measured within the thermal energy range. In all these systems the main ionic product is the

Hg^+ atomic ion, while the associate ion is produced with a relative yield of only a few percent, in the case of metastable neon, and ranging from $\sim 20\%$ to $\sim 30\%$ in the case of metastable krypton and argon.

The associative to total ionization branching ratio decreases monotonically as a function of the collision energy for metastable argon, while data for the metastable krypton exhibit two changes in slope. The shape of the energy dependence of the branching ratio for metastable argon appears similar to those of other cases previously reported.[9,10,33-35] In the case of metastable krypton the unusual trend of the branching ratio, with a minimum around 0.15 eV[5] and a maximum around 0.5 eV, has to be attributed to the different role played by the two spin–orbit states of the metastable atoms in the ionization processes of mercury. The $^3P_0$ state can produce both atomic and associate ions in the whole experimentally investigated energy range, as in the metastable argon atom case. On the other hand, the $^3P_2$ state leads to ionization only at an energy higher than ~ 0.15 eV. This threshold energy is smaller than expected, from the potential energy curves of Kr*–Hg and Kr–Hg^+, indicating the possibility of a nonadiabatic coupling with Kr–Hg** states before the transition to the ionization continuum.

The experimental results have been analyzed in terms of the usual optical model. This model appears to be rather adequate to describe the present results for Ne*, Ar*, and Kr*($^3P_0$)–Hg systems. In the Kr*($^3P_2$)–Hg system the presence of a manifold of nonadiabatically coupled channels which can penetrate the ionization continuum leads to the failure of the model.

ACKNOWLEDGMENTS

The authors wish to thank V. Aquilanti and S. Cavalli for helpful discussions on some theoretical aspects and G. Liuti and F. Pirani for a critical reading of the manuscript. Partial financial support by Philips Research Laboratory, Eindhoven, The Netherlands, is gratefully acknowledged.

[1]Z. Herman and V. Cermak, Collect. Czech. Chem. Comm. **28**, 799 (1963).
[2]E. Illenberger and A. Niehaus, Z. Phys. B **20**, 33 (1975).
[3]H. Hotop, J. Lorenzen, and A. Zastrow, J. Electron Spectrosc. Relat. Phenom. **23**, 347 (1981).
[4]A. J. L. Burgmans and A. H. M. Smeets, J. Phys. D **16**, 755 (1983); A. J. L. Burgmans and H. J. M. Merks-Eppingbroek, *ibid.* **17**, 1159 (1984).
[5]L. Appolloni, B. Brunetti, J. Hermanussen, F. Vecchiocattivi, and G. G. Volpi, Chem. Phys. Lett. **129**, 287 (1986).
[6]W. Lee and R. M. Martin, J. Chem. Phys. **64**, 678 (1976).
[7]D. J. Wren and D. W. Setser, J. Chem. Phys. **74**, 2331 (1981).
[8]A. Aguilar-Navarro, B. Brunetti, M. Cardinalini, F. Vecchiocattivi, and G. G. Volpi, Gazz. Chim. Ital. **113**, 711 (1983).
[9]A. Aguilar-Navarro, B. Brunetti, S. Rosi, F. Vecchiocattivi, and G. G. Volpi, J. Chem. Phys. **82**, 773 (1985).
[10]B. Brunetti, F. Vecchiocattivi, and G. G. Volpi, J. Chem. Phys. **84**, 536 (1986).
[11]H. Nakamura, J. Phys. Soc. Jpn. **26**, 1473 (1969).
[12]W. H. Miller, J. Chem. Phys. **52**, 3563 (1970).
[13]H. Nakamura, J. Phys. Soc. Jpn. **31**, 874 (1971).
[14]H. Nakamura, J. Phys. Soc. Jpn. **33**, 1426 (1972).
[15]S. E. Nielsen and J. S. Dahler, J. Chem. Phys. **71**, 1910 (1979).
[16]A. Niehaus, Adv. Chem. Phys. **65**, 399 (1981).
[17]J. N. L. Connor and A. D. Smith, Mol. Phys. **43**, 397 (1981); J. Chem. Phys. **78**, 3161 (1983); and references therein.
[18]F. Vecchiocattivi, Comments At. Mol. Phys. **17**, 163 (1986).
[19]V. Aquilanti, E. Luzzatti, F. Pirani, and G. G. Volpi, Chem. Phys. Lett. **90**, 382 (1982); P. Casavecchia, G. He, R. K. Sparks, and Y. T. Lee, J. Chem. Phys. **77**, 1878 (1982); V. Aquilanti, F. Pirani, and F. Vecchiocattivi (to be published).
[20]U. Buck and H. Pauly, J. Chem. Phys. **54**, 1929 (1971).
[21]U. Lackschwitz, J. Maier, and H. Pauly, J. Chem. Phys. **84**, 343 (1986).
[22]U. Buck, M. Kick, and H. Pauly, J. Chem. Phys. **56**, 3391 (1972).
[23]P. Barwig, U. Buck, E. Hundhausen, and H. Pauly, Z. Phys. **196**, 343 (1966).
[24]N. J. Bridge, J. Mol. Spectrosc. **42**, 370 (1972).
[25]S. H. Linn, J. M. Brom, W. B. Tzeng, and C. Y. Ng, J. Chem. Phys. **82**, 648 (1985).
[26]C. L. Liao and C. Y. Ng, J. Chem. Phys. **84**, 1142 (1986).
[27]G. Liuti and F. Pirani, Chem. Phys. Lett. **122**, 245 (1985).
[28]R. W. Gregor and P. E. Siska, J. Chem. Phys. **74**, 1078 (1981).
[29]P. M. Dehmer, Comments At. Mol. Phys. **13**, 205 (1983).
[30]The value of the quenching rate constant for Ar* in Hg is obtained by combining those reported in Ref. 7 for Ar*($^3P_2$) and Ar*($^3P_0$) accordingly the statistical population of these two J states in our experiment.
[31]C. F. Moore, *Atomic Energy Levels* (U.S. GPO, Washington, D.C., 1958), Vol. 3, p. 469.
[32]W. H. Miller and H. Morgner, J. Chem. Phys. **67**, 4927 (1977).
[33]A. Pesnelle, G. Watel, and C. Manus, J. Chem. Phys. **62**, 3590 (1975).
[34]R. H. Neynaber and G. D. Magnuson, Phys. Rev. A **14**, 961 (1976).
[35]R. H. Neynaber and S. Y. Tang, J. Chem. Phys. **70**, 4272 (1979).